Target Detection and Tracking via Sparsity-Promoting Tikhonov Regularization

Sergey Fridman†, L.J. Nickisch†, Mark Hausman†, Michael Matthews†

† NorthWest Research Associates, Monterey, CA

***Abstract*—We discuss the utilization of sparsity-promoting regularization within the SIFTER target detection capability for OTH radar. SIFTER combines ionospheric modeling and ray tracing to detect small-RCS targets in noise and clutter. The SIFTER solution is interpreted as the distribution of backscatter cross section in ground coordinates (scattering surface). Solutions are obtained by solving the inverse problem with Tikhonov regularization. The utilization of concepts of sparsity-promoting regularization with fractional norms helps to combine multimode target returns into an single enhanced peak on the scattering surface, the position of which provides a high-fidelity estimate of target geolocation.**

I. Introduction

Over-the-Horizon Radar (OTHR) uses ionospheric reflection to propagate HF transmissions over long distance [1]. Detection, tracking, and geolocation of OTHR targets requires real-time, high-fidelity channel information to convert target signal delays and transmit/receive beam angles into decision statistics and geolocation estimates. A high-fidelity HF channel model that supports precise ray-tracing and prediction of all radar propagation modes also incorporates multimode detection of known targets. An ionospheric model with ray-tracing codes combines with a novel target detection capability called SIFTER (Signal Inversion For Target Extraction and Registration) to achieve enhanced target detection and tracking in ground coordinates, rather than in the usual domain of radar-measured delay and beam angles [5]. This paper augments ground-space SIFTER processing with sparsity-promoting regularization. The utilization of mathematical concepts of sparsity and fractional norms permits the combination of multimode target returns into an single enhanced peak close to the true target geolocation.

Ray tracing propagation simulation is provided by the CREDO (Coordinate Registration Enhancement by Dynamic Optimization) software package [3]. The ionospheric model for ray tracing is furnished by the GPSII (GPS Ionospheric Inversion) software package. GPSII is an ionospheric data assimilation capability that produces real-time three-dimensional ionosphere models using GPS beacon data, ionogram-derived electron density profiles, as well as known OTHR targets [2].

SIFTER facilitates the detection of small-RSC targets in noise and clutter by solving the inverse problem of distributed scatterers that best reproduce the radar measurements [5], [6], [7]. Non-coherent radar measurements are represented by the Amplitude-Range-Doppler (ARD) map. Coherent radar measurements comprise a time series of in-phase and quadrature (IQ) samples measured at the receiver. The SIFTER inverse solution uses the Tikhonov regularization smoothing constraint [4] to suppress clutter sources in the scattering volume while maximizing target returns. Solutions evolve in time to smooth spurious noise sources that do not evolve consistently with their Doppler velocity.

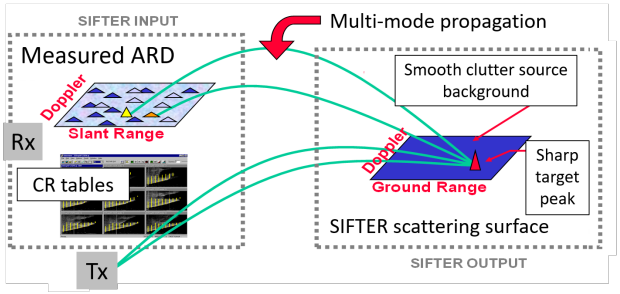

Fig. 1: SIFTER determines the smoothest distribution of scatterers consistent with measured ARD. Targets appear as sharp peaks whereas clutter sources are more broadly distributed.

Figure 1 illustrates the SIFTER concept wherein the radar returns consist of waves backscattered by objects in the area of illumination. The received power as a function of radar coordinates and Doppler shift may be expressed as an integral operator applied to the backscatter cross section σ on the Earth's surface. In general, σ is a function of both the geographic location and the scatterer's velocity vector. Targets appear in σ as delta-function-like peaks. The kernel of the integral operator is treated as a known function that is determined entirely by a model of the propagation channel, antenna

patterns, and radar signal processing parameters. The relationship between σ and the received power is an integral equation to be solved (inverted) with respect to σ. This inverse solution uses Tikhonov regularization for ill-posed problems. The solution for scattering surface σ is analyzed for peaks, the location of which provides an estimate of the actual coordinates and velocity vector of the target. SIFTER processing provides a sensitivity gain due primarily to the time evolution algorithm. Introduced here is a continuity equation for σ based on general assumptions regarding the behavior of potential targets. This equation evolves surface σ between radar revisit cycles. The data from each subsequent revisit are used to correct σ evolved from previous cycles. This helps the SIFTER inversion to recover targets that experience irregular fading and to minimize the effects of spurious noise-related peaks.

Instead of threshold-based peak-picking of individual returns in ARD space, the SIFTER method exploits channel information and radar antenna patterns to interpret the complete radar return (clutter, noise, and targets) for the entire radar search area by solving for the distribution of scatterers σ that reproduces the measured returns. The time evolution of SIFTER solutions provides the greatest gain. Spurious noise peaks that do not evolve consistently with their Doppler velocity are quickly attenuated, thereby exposing weak targets.

II. Overview of SIFTER

A. Continuity Equation

Sensitivity gain is achieved by accumulating the SIFTER solution in time using a Kalman filter, where the entire scattering surface is treated as the state vector of the observed dynamic system. The SIFTER solution assumes that target cross sections vary slowly in time along a trajectory $\mathcal{T}$,

$$\left(\frac{d}{dt}\,\sigma\right)_{\mathcal{T}} \;=\; 0\,. \tag{1}$$

Position and velocity vectors characterize the dynamical state and short-term motion of the target. For tracking the evolution of scattering surface σ, we assume that it is a function of range ρ, azimuth ϕ, range rate ν_ρ, and azimuth rate ν_ϕ, i.e., $\sigma = \sigma(\rho, \phi, \nu_\rho, \nu_\phi)$.

The total time derivative of scattering surface σ along trajectory $\mathcal{T}$ becomes,

$$\left(\frac{d}{dt}\,\sigma\right)_{\mathcal{T}} = \frac{d\sigma}{dt} + \nu_\rho\,\frac{d\sigma}{d\rho} + \nu_\phi\,\frac{d\sigma}{d\phi} + a_\rho\,\frac{d\sigma}{d\nu_\rho} + a_\phi\,\frac{d\sigma}{d\nu_\phi} \tag{2}$$

where a_ρ and a_ϕ are the respective acceleration components.

For the majority of surface radar applications there is no explicit relationship between target state vector $(\rho, \phi, \nu_\rho, \nu_\phi)$ and target acceleration (a_ρ, a_ϕ). Because surface targets often change state in an unpredictable manner, we treat the acceleration terms in (2) as random processes. Acceleration information could be included in (2) to filter those targets with a specified acceleration. Expressions (1) and (2) combine to yield a continuity equation of the form,

$$\frac{d\sigma}{dt} \;+\; \nu_\rho\,\frac{d\sigma}{d\rho} \;+\; \nu_\phi\,\frac{d\sigma}{d\phi} \;+\; \sigma/\tau \;=\; \eta\,, \tag{3}$$

where τ is the relaxation time, and where $\eta = \eta(t, \rho, \phi, \nu_\rho, \nu_\phi)$ represents random scatterers, including targets that change state and scattering cross section in an unpredictable manner. Relaxation parameter τ limits the update period in which a predicted target trajectory is valid.

Equation (3) postulates a model of target dynamics, in which a target may exist at any point in ground space, may move in all directions with all possible velocities, and may possess an arbitrary scattering cross section. The target scattering properties evolve according to

$$\frac{d\sigma}{dt} \;+\; \sigma/\tau \;=\; \eta\,, \tag{4}$$

where, in practice, the attenuation time constant τ is relatively large, while the variance of random source η is small. Equation (4), which governs the evolution of scattering surface σ, can be solved using the Method of Characteristics. Given the state of scattering surface $\sigma(t_0, \rho, \phi, \nu_\rho, \nu_\phi)$ at time t_0, the surface at $t > t_0$ may be expressed as

$$\begin{aligned}\sigma(t, \rho, \phi, \nu_\rho, \nu_\phi) = \\ \sigma(t_0,\, \rho - (t-t_0)\nu_\rho,\, \phi - (t-t_0)\nu_\phi,\, \nu_\rho,\, \nu_\phi) \\ \cdot\, e^{-(t-t_0)/\tau} \;+\; \bar{\eta}\end{aligned} \tag{5}$$

where $\bar{\eta}$ is the random component of σ,

$$\begin{aligned}\bar{\eta} \;= \\ \int_{t_0}^{t} \eta(s,\, \rho - (s-t_0)\nu_\rho,\, \phi - (s-t_0)\nu_\phi,\, \nu_\rho,\, \nu_\phi) \\ \cdot\, e^{-(t-s)/\tau}\, ds\end{aligned} \tag{6}$$

B. Tracking the Scattering Surface

The relationship between the scattering surface and the radar measurements along with the continuity equation in (5) provide the framework for formulating the tracking problem of scattering surfaces in the form of a discrete-

time Kalman-Filter, in which the nth radar revisit is expressed as

$$Y(\rho_s,\phi_s,\nu_D) \;=\; \iint M(\rho_s,\phi_s,\nu_D,\rho,\phi,\nu_\rho,\nu_\phi) \cdot \sigma(\rho,\phi,\nu_\rho,\nu_\phi)\cdot d\rho\; d\phi\; d\nu_\rho\; d\nu_\phi + \chi_n(\rho,\phi,\nu_\rho,\nu_\phi) \quad (7)$$

and

$$\sigma_n(\rho,\phi,\nu_\rho,\nu_\phi) \;= \sigma_{n-1}(t_0,\rho-\nu_\rho\,\delta t,\phi-\nu_\phi\,\delta t,\nu_\rho,\nu_\phi)\; e^{-\delta t/\tau} + \eta_n(\rho,\phi,\nu_\rho,\nu_\phi) \quad (8)$$

where $Y(\rho_s,\phi_s,\nu_D)$ is the observed signal for the range-azimuth-Doppler bin specified by parameters ρ_s, ϕ_s, and ν_D. Terms $\chi_n(\rho,\phi,\nu_\rho,\nu_\phi)$ and $\eta_n(\rho,\phi,\nu_\rho,\nu_\phi)$ correspond, respectively, to measurement noise within interval $\delta t = t_n - t_{n-1}$ and random noise in continuity Equation (3). Equation (7) incorporates the dependence of the scattering surface on the velocity components and the dependence of received power on Doppler velocity ν_D. Kernel $M(\rho_s,\phi_s,\nu_D,\rho,\phi,\nu_\rho,\nu_\phi)$ describing ionospheric propagation is considered here to be a known function. Also known is time constant τ and certain statistical characteristics of noise term $\chi_n(\rho,\phi,\nu_\rho,\nu_\phi)$ and target maneuvering term $\eta_n(\rho,\phi,\nu_\rho,\nu_\phi)$.

The crucial element of the SIFTER analysis is estimating (tracking) scattering surface σ_n, on which discrete targets form as peaks. An advanced procedure for estimating σ_n utilizes observation time series $(Y_n, Y_{n-1}, \ldots)$, the relationship between σ_n and the observations in (7), and knowledge of the evolution of σ_n in (8).

C. Comparison with Track-Before-Detect

SIFTER is similar to Track-Before-Detect (TBD) algorithms [8] in extracting weak target signals from noise. TBD algorithms hypothesize possible target trajectories (tracks), then use observations to accumulate track likelihoods based on signal strength along the track's projection in radar coordinates. Tracks with sufficient likelihoods are declared valid. In comparison, SIFTER reconstructs and tracks an evolving scattering surface, creating a radar response that matches the radar data in the entire radar field of view. Localized targets form distinct peaks on the evolving scattering surface, which grow more distinct as tracking progresses.

SIFTER differs from TBD by replicating the entire radar response, whereas TBD associates individual radar cells with hypothetical tracks. SIFTER imposes no limit on the number of targets, processing multiple targets in the same manner and with the same computational load as a single target. TBD algorithms hypothesize the number of possible targets before processing, and computational load increases with the number of targets.

III. Sparsity-Promoting SIFTER

The SIFTER solution in (7) solves the following integral equation within each time step n.

$$Y(\rho_s,\phi_s,\nu_D) \;\approx\; \iint M(\rho_s,\phi_s,\nu_D,\rho,\phi,\nu_\rho,\nu_\phi) \cdot \sigma(\rho,\phi,\nu_\rho,\nu_\phi)\cdot d\rho\; d\phi\; d\nu_\rho\; d\nu_\phi \quad (9)$$

Here $\sigma = \sigma(\rho,\phi,\nu_\rho,\nu_\phi)$ is the scattering surface (the field of the backscatter cross section) as a function of the ground range ρ, azimuth ϕ, range rate ν_ρ, and azimuth rate ν_ϕ. The vector $Y(\rho_s,\phi_s,\nu_D)$ of ARD measurements, which is a function of slant range ρ_s, slant azimuth ϕ_s, and the Doppler velocity ν_D, is the kernel that is estimated based on both the ground-to-slant mapping operator as well as radar beam forming, range, and Doppler processing. The approximation in (9) means that Equation (7) need be satisfied only to within measurement accuracy.

The Tikhonov method offers a robust procedure for building a stable solution of the inverse problem in (9), rewritten as

$$Y = M\sigma + \chi\;, \quad (10)$$

where Y is a known measurement vector, and where χ is a random noise vector with covariance matrix $S = \langle \chi\chi' \rangle$. The dimension of vector σ exceeds that of measurement vector $(\dim\sigma > \dim Y)$. The regularized solution postulates a symmetric positive-definite matrix P with $\operatorname{rank} P = \dim\sigma$ and quadratic form $\Omega[\sigma] = \sigma' P^{-1}\sigma$ called the stabilizer or stabilizing functional. The regularized solution σ satisfies the condition

$$\frac{1}{\dim Y}\,(Y - M\bar\sigma)'\,S^{-1}\,(Y - M\bar\sigma) \;\le\; 1 \quad (11)$$

and minimizes stabilizer

$$\Omega[\sigma] \to \min\;. \quad (12)$$

Condition (11) means that the error of the fit provided by $\bar\sigma$ is consistent with measurement errors characterized by S.

Quadratic form (11) is closely related to the l_2 norm of vector σ in that $\Omega[\sigma] = l_2^2[Q\sigma]$, for any $Q = (P^{-1})^{1/2}$. Replacing l_2-based stabilizers with l_p-based stabilizers $(p \le 1)$ is beneficial for problems that have sparse solutions [9]. Here norm l_p is defined for any vector $x = (x_1, x_2, \ldots, x_N)$ in the usual manner, $l_p[x] = (\sum_n |x_n|^p)^{1/p}$.

Because scattering surface σ contains only a few target peaks, we consider the utility of l_p–based stabilizers for the SIFTER inverse problem. More generally, we are

interested in solving the problem posed in (10), where the stabilizing functional Ω is defined in terms of the l_p norm for arbitrary $p > 0$, i.e.,

$$\Omega[\sigma] = (l_p[\sigma])^p = l_p^p[\sigma], \qquad p > 0\ . \tag{13}$$

Optimization schemes utilizing l_p with $p \neq 2$ are known to be very computationally expensive, with the exception of the case $p = 1$, which can be solved efficiently via linear programming. A robust algorithm was developed that approximates the solution to (11) and (12) for reasonable values of $p > 0$. This algorithm is based on experience in solving nonlinear inverse problems and, in particular, inverting ionospheric measurement data, such as backscatter soundings and total electron content measurements, for OTH radar diagnostics [10].

The optimization approach transforms the underlying linear equation in (9) into a nonlinear equation such that stabilizer (13) becomes a quadratic form. The optimization problem in (11) and (12) then reduces to a nonlinear least-squares problem, which is efficiently solved via Gauss-Newton algorithm. In other words, vector σ is replaced with new vector u using the one-to-one mapping

$$\sigma = \Phi(u)\ , \tag{14}$$

such that

$$l_p^p[\Phi(u)] = l_2^2[u]\ . \tag{15}$$

Then the problem in (10) is transformed into

$$\frac{1}{\dim Y}\,(Y - \Psi u)'\,S^{-1}\,(Y - \Psi u)\ \leq\ 1 \tag{16}$$

$$u'\,u\ \rightarrow\ \min \tag{17}$$

where nonlinear operator Ψ is defined as

$$\Psi\,u = M\,\Phi(u)\ . \tag{18}$$

Consider, for example, the one-to-one transformation Φ : $\sigma_n = u_n(u_n^2)^{1/p-1/2}$ that satisfies (15). Here u_n and σ_n are respective components of vectors u and σ, such that Φ could be employed for $0 < p \leq 2$. However, this transformation makes it difficult to use Newton-type iterative methods because the inverse transformation is not differentiable. We employ the following modification of this transformation

$$\Phi_\epsilon : \sigma_n = u_n(|u_n|^2 + \epsilon^2)^{1/p-1/2} \tag{19}$$

where $\epsilon > 0$ is a user-defined parameter. This transformation possesses desired differentiability properties and Φ_ϵ can satisfy (15) to within any desired accuracy ϵ. In the following examples, parameter ϵ is orders of magnitude smaller than any discernible target solution, meaning that the stabilizer defined by relationships (14), (17), and (19) provides a good approximation to l_p-norm-based stabilizer. The parameterization in (19) is applicable to both real- and complex-valued data.

Figure 2 shows an example of an Amplitude-Range-Doppler (ARD) map measured by ROTHR Virginia, representing 16 consecutive beams with 0.47-degree separation. Beam 11 contains a multimode return from an unknown target. A CREDO-KRP model of the ionosphere for this date and time was generated by employing WSBI, QVI, and multimode transponder data. The model performed ray-tracing and generated SIFTER kernel M in (7) for three consecutive dwells. Figure 3 compares

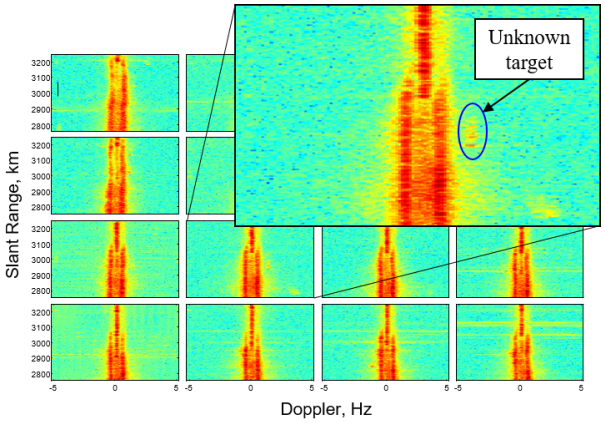

Fig. 2: Single-dwell ROTHR amplitude-range-Doppler (ARD) data for finger-beams 2 through 17. A multimode return from an unknown target is visible in Beam 10.

solutions obtained in the vicinity of the target after processing the first dwell. Figure 3 (left) shows the solution obtained using the conventional l_2 stabilizer in **??**) with P the identity matrix, and the ground range/ground azimuth layer at the estimated velocity vector of the target (radial velocity of –9.6 m/s and zero azimuth velocity). A strong peak is visible at range 2751.2 km and azimuth 163.7 degrees, spread over 3 km in range and 0.5 degrees in azimuth. Numerous secondary peaks, which are attenuated more than 12 dB, are likely caused by both noise and propagation modeling error. Figure 3 (center) shows the solution for the same data obtained with the l_1 stabilizer, where the main peak is better localized, while secondary peaks are fewer and weaker (–18 dB or more). Figure 3 (right) shows the solution for the same data with the $l_{1/2}$ stabilizer, where the localization of the main peak is further improved to just a single spatial solution cell (0.7 km in range and 0.25 degrees in azimuth). There is only one discernible secondary peak attenuated by 27 dB.

Thus, the benefit of utilizing the sparsity-promoting regularization within SIFTER appears to be two-fold.

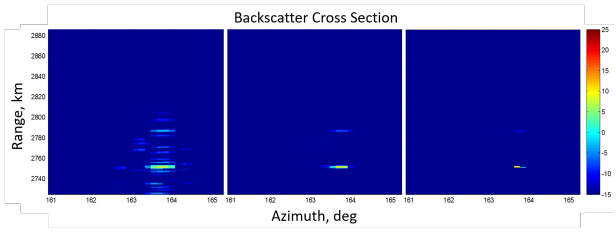

Fig. 3: Range-azimuth layer of SIFTER solutions at a fixed velocity vector in the vicinity of the target indicated in Figure 2 after processing of the first dwell. Left, center, and right figures use stabilizers l_2, l_1, and $l_{1/2}$, respectively.

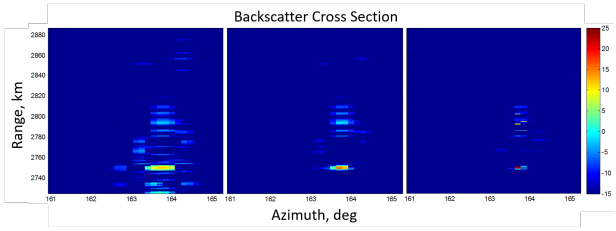

Fig. 4: Range-azimuth layer of SIFTER solutions at a fixed velocity vector in the vicinity of the target, indicated in Figure 2 after processing three consecutive dwells. Left, center, and right figures use stabilizers l_2, l_1, and $l_{1/2}$, respectively.

The first benefit is that target peaks on the scattering surface become sharper. The second benefit is that multiple modes combine into a single distinct peak on the scattering surface.

Figure 4 shows the same solutions as in Figure 3 obtained after accumulating three consecutive dwells of data. The localization properties of main target peak in each solution remain unchanged while the magnitude of the peak increases by 3 dB in the l_2-norm case, by 5 dB in the l_1 case, and 9 dB in the $l_{1/2}$ case. Multiple secondary peaks are noticeable in every solution. The secondary peaks are attenuated by no less than 10 dB, 18 dB, and 15 dB, respectively, for the l_2, l_1, and $l_{1/2}$ stabilizers. SIFTER processing of the first dwell of data amounts to inversion of the slant space data into the ground space. The operator being inverted is obtained using ray-tracing and it provides the mapping of scatterers from ground space into slant space. Measurement noise, uncertainties of the ionospheric model and the ray tracing as well as inherent non-uniqueness of the inverse problem inevitably cause uncertainties in the solution. In the case of multimode propagation the most noticeable manifestation of these uncertainties are secondary peaks in the solution which can be interpreted as misidentified modes. The promotion of sparseness associated with l_p-based stabilizers ($p \leq 1$) gives stronger preference to solutions with fewer sources thus reducing or eliminating secondary peaks in the solution. All three solutions shown in Figure 3 employ the same ground-to-slant space mapping operator and fit the same data equally well, but the solution employing the $l_{1/2}$ stabilizer produces the most sensible interpretation of the data.

Subsequent steps of SIFTER processing involve advancement of the solution estimate to the time of the next dwell using the continuity equation (3) with $\eta = 0$ [7], and updating the solution with new data using the relationship in (8). In the case of the l_2 stabilizer, the main peak becomes localized within a single solution cell causing considerable interpolation errors on subsequent time steps. It is likely that these interpolation errors are causing amplification of the secondary peaks in this case. In response to this issue, we are developing generalizations of l_p regularization that restrict the degree of localization.

IV. Conclusion

The SIFTER algorithm for inverting radar data into ground space was extended to utilize sparsity-promoting regularization instead of the l_2 regularization employed earlier. We conclude that the sparsity-promoting regularization better reflects the nature of the desired behavior of the scattering surface associated with a number of localized targets. In addition, this regularization is beneficial in the presence of multi-mode propagation channels. Regularization enables automatic interpretation of multimode signals in terms of the fewest number of targets.

We developed an original method for obtaining approximate l_p-regularized solutions. This method is based on approximate mapping of the l_p-regularized problem onto a nonlinear l_2-regularized problem, which is then solve using algorithms that we developed earlier for ionospheric inversion.

References

[1] K. Davies, *Ionospheric Radio*, Peter Peregrinus Ltd., London, United Kingdom, 1990.

[2] S.V. Fridman, L.J. Nickisch, M.A. Hausman, G. Zunich. "Assimilative Model for Ionospheric Dynamics Employing Delay, Doppler, and Direction of Arrival Measurements from Multiple HF Channels: Assimilation of HF Measurements," *Radio Science*, Vol. 51, No. 3, March 2016.

[3] L.J. Nickisch, S.V. Fridman, M.A. Hausman, "Fully automated three-dimensional ionospheric reconstruction from OTH radar soundings," *Proceedings of the Ninth Annual Ionospheric Effects Symposium*, edited by J. M. Goodman, pp. 607618, Natl. Telecommun. and Inf. Serv., Alexandria, Va., 1999.

[4] A.N. Tikhonov, V.Y. Arsenin, *Solution of Ill-Posed Problems*, Halsted, New York, 1977.

[5] L.J. Nickisch, S.V. Fridman, M. A. Hausman, "SIFTER: Signal Inversion For Target Extraction and Registration Proof of Concept," *Interim technical report for Contract F30602-00-C-0162*, Mission Research Corporation MRC/MRY-R-111, July 2001.
[6] L.J. Nickisch, S.V. Fridman, M.A. Hausman, "SIFTER: Signal Inversion For Target Extraction and Registration Coherent Processing of IQ Data," *Final report for Contract F30602-00-C-0162*, Mission Research Corporation MRC/MRY-R-111, July 2003.
[7] S. Fridman, L.J. Nickisch, "SIFTER: Signal inversion for target extraction and registration," *Radio Science*, Vol. 39, No. 1, 2004.
[8] S. Blackman, R. Popoli, *Design and Analysis of Modern Tracking Systems*, Norwood, MA: Artech House, 1999.
[9] M. Elad, *Sparse and Redundant Representations*, Springer, 2010.
[10] S.V. Fridman, L. J. Nickisch, M.A. Hausman, "Inversion of backscatter ionograms and TEC data for over-the-horizon radar," *Radio Science*, Vol. 47, 2012.